Chinese Journal of Oceanology and Limnology
Vol. 30 No. 6, P. 1068-1081, 2012
http://dx.doi.org/10.1007/s00343-012-1275-8

Numerical simulation of the structure and variation of upwelling off the east coast of Hainan Island using QuikSCAT winds*

LI Yineng (李毅能), PENG Shiqiu (彭世球)**, YANG Wei (杨威), WANG Dongxiao (王东晓)

Key Laboratory of Tropical Marine Environmental Dynamics, South China Sea Institute of Oceanology, Chinese Academy of Sciences, Guangzhou 510301, China

Received Dec. 18, 2011; accepted in principle Jan. 29, 2012; accepted for publication Apr. 8, 2012

Abstract The spatial structure and variation of the upwelling in the waters east and northeast of Hainan Island, China during 2000–2007 were investigated using a nested high-resolution Princeton Ocean Model (POM) forced by QuikSCAT winds. The model produced good simulations of the summer upwelling and the seasonal and annual variability. Strong upwelling occurs from mid-July to mid-August with a peak east of Hainan Island associated with the southwesterly monsoon in the South China Sea. Sensitivity experiments indicated that when the local wind stress controls the variability of the upwelling, the large-scale circulation significantly enhances the upwelling northeast of Hainan Island by inducing a local upwelling and transporting cold water northeast-ward along the island's east coast. The joint effects of the local wind stress and large-scale circulation result in stronger upwelling northeast of Hainan Island. This implies that the annual variation of the upwelling northeast of Hainan Island is controlled not only by the local alongshore wind stress but also by the large-scale circulation. This result will help us investigate the decadal variation of the upwelling in this region in the future.

Keyword: upwelling; high-resolution nested model; South China Sea; QuikSCAT winds

1 INTRODUCTION

In coastal oceans, wind-induced upwelling or downwelling is a common phenomenon (Ekman, 1905). Most coastal upwelling systems thus vary according to the time scales of the wind stress variability. The inter-seasonal and inter-annual variability of the upwelling are important issues affecting the variability of biological productivity. For example, the Peruvian upwelling system varies with the intensity of the trade winds that weaken or reverse during El Niño years, resulting in a significant decline of fish stock along the Peruvian coast (Barber et al., 1985).

The South China Sea (SCS) is the largest marginal sea in the tropics with a maximum depth of more than 5 000 m (Fig.1a). It covers an area from the equator to 23°N and from 99°E to 121°E, and borders the East China Sea in the northeast, the Pacific Ocean and the Sulu Sea in the east, and the Java Sea and the Indian Ocean in the southwest. Climatic variations in the atmosphere and in the upper layer of the ocean in the SCS are dominated by the East Asian monsoon system (Wyrtki, 1961; Su, 2004). The southwest summer monsoon lasts from June through September. The stronger northeast winter monsoon occurs from November to March and varies with the Southern Oscillation Index (Liu et al., 2002).

Hainan Island is the largest island in the SCS, located in the northwest of the SCS (Fig.1a, b). Coastal upwelling in the northern SCS (NSCS), especially in the Hainan coastal areas, has gained

* Supported by the Knowledge Innovation Program of Chinese Academy of Sciences (Nos. KZCX2-YW-Q11-02, KZCX2-EW-208), the One Hundred Talent Program of Chinese Academy of Sciences, the National Natural Science Foundation of China (No. 41076009), and the Youth Frontier Science Project of the South China Sea Institute of Oceanology (No. SQ200914)
** Corresponding author: speng@scsio.ac.cn

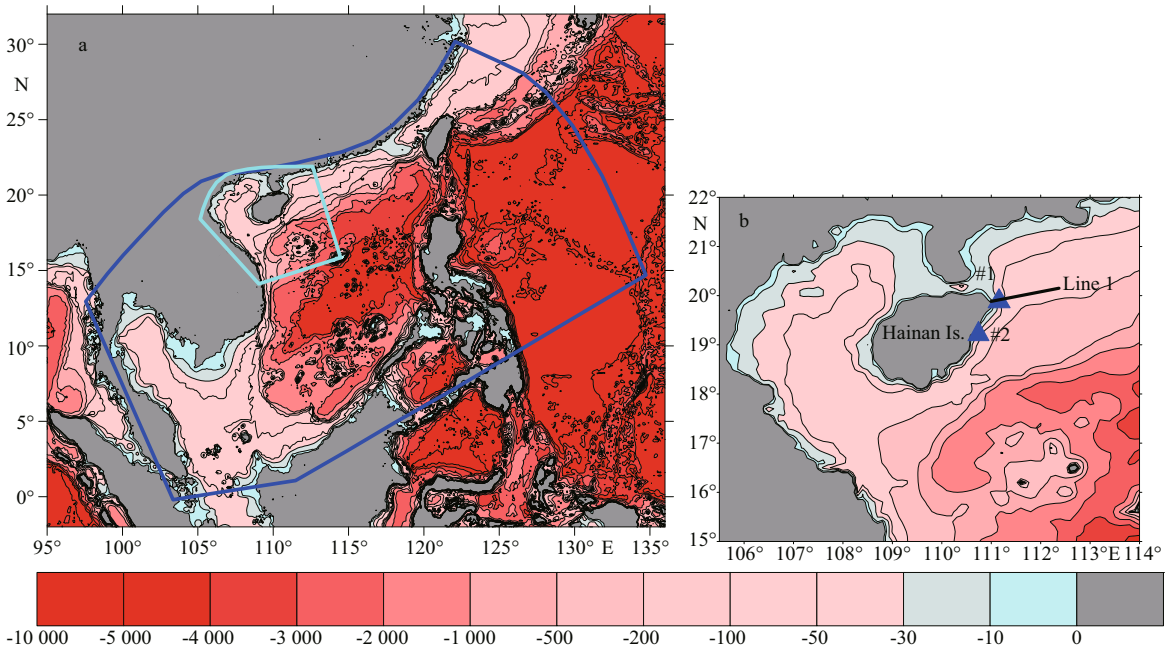

Fig.1 a. Bathymetry (m) of the South China Sea and the configuration of the nested model domains; b. bathymetry of the inner domain

considerable attentions. Summer upwelling off the east coast of Hainan Island and southern Shantou city was first noticed by Niino and Emery (1961). Early investigations can be traced back to the 1960s (Guan and Chen, 1964). Using observations and a two-dimensional diagnostic model, Gou et al. (1998) calculated the maximum vertical velocity to be 3.21×10^{-5} m/s at a depth of 30 m, 10 km offshore. Chai et al. (2001) studied the dynamics and inter-annual variability of the upwelling and its relation to the ecosystem along the east coast of Hainan Island. Li (1990; 1993) and Hong and Li (1991) analyzed 20-year data of water temperature, salinity, and dissolved oxygen in the NSCS. Their results suggest that the summer upwelling in the NSCS is a common seasonal phenomenon with a basin-scale spatial extent. This has been confirmed in recent numerical simulations (Jing, 2009).

The dynamic mechanism of the NSCS upwelling is complex. The upwelling variability involves many factors including wind stress, bottom topography, large-scale circulation, and eddies. Previous studies have suggested that the center of the upwelling lies in the area east and northeast of Hainan Island (Han et al., 1990; Li, 1990; Deng and Zhong, 1995; Chai et al., 2001; Jing et al., 2009). The upwelling was found to be correlated with the large-scale circulation in the SCS (Deng and Zhong, 1995; Su, 2009). Jing et al. (2009) used the Estuarine Coastal Ocean Model (ECOM) to simulate 3-D structures of the upwelling and found that Ekman pumping induced by wind stress curls also plays an important role in the upwelling in the region. All these studies provide a preliminary scenario of the structure and mechanism of the upwelling. However, some major questions remain unanswered. For example, how does coastal upwelling respond to the inter-annual variability of the monsoon winds? When does the intensity of the upwelling reach its peak during the summer? Furthermore, according to the Ekman theory, when the southwesterly winds prevail in summer, the main center of the upwelling should appear in the waters east of Hainan Island. However, strong upwelling is frequently observed northeast of the island. Therefore, it is of interest to theoretically explore the differences in the dynamic mechanism and inter-annual variations of the upwelling to gain answers to these questions which are of great importance for the management and protection of fishery resources and environments.

2 OBSERVATIONS OF UPWELLING EAST AND NORTHEAST OF HAINAN ISLAND

Generally, the upwelling process wells up cold, nutrient-rich water of high salinity from the deep layers to the surface. The upwelling phenomena can

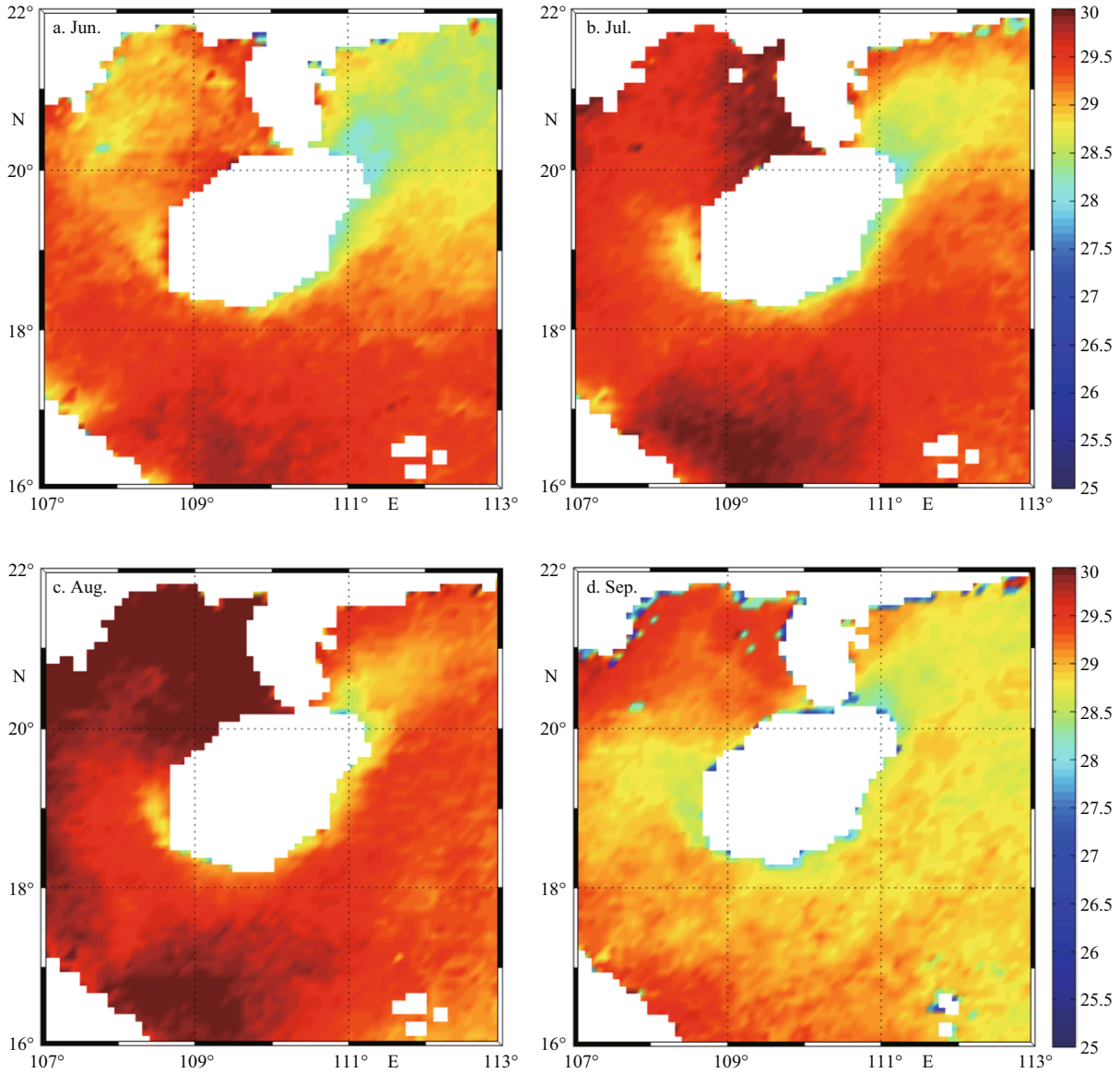

Fig.2 The climatological monthly-mean NOAA AVHRR SSTs (°C) around Hainan Island for (a) June, (b) July, (c) August, and (d) September

be inferred from sea surface temperature (SST) measurements by the Advanced Very High Resolution Radiometer (AVHRR) on board the satellites of the National Oceanic and Atmospheric Administration (NOAA). We used a climatological monthly-mean SST dataset, which was created using daily Pathfinder SSTs from 1985 to 2002 with a spatial resolution of 9.28 km. Summer SSTs around Hainan Island from June through September (Fig.2) show cold water centers on the surface east and northeast of Hainan Island with peaks in June and July in the sea northeast of the island.

Figure 3 shows the MODAS (Modular Ocean Data Analysis System) (Kara and Barron, 2007) SSTs observed in July of 2003 to 2008. The SST dataset used here was derived from the MODAS Aqua Satellite mapped products (http://oceandata.sci.gsfc.nasa.gov/MODISA/Mapped/) for 2003–2008 with a spatial resolution of 4 km. In July of 2003–2008, cold water with SSTs 1–2°C lower than the surrounding temperature is clearly seen along the east coast of Hainan Island and extending northeastward.

The upwelling can also be detected by Conductivity Temperature Depth (CTD) observations. Here, we use the observations collected during the '908' Special Marine Survey from Jul. 19 to Aug. 5, 2006. The horizontal temperature distribution, which was plotted using the Cubic Spline Interpolation method (Fig.4),

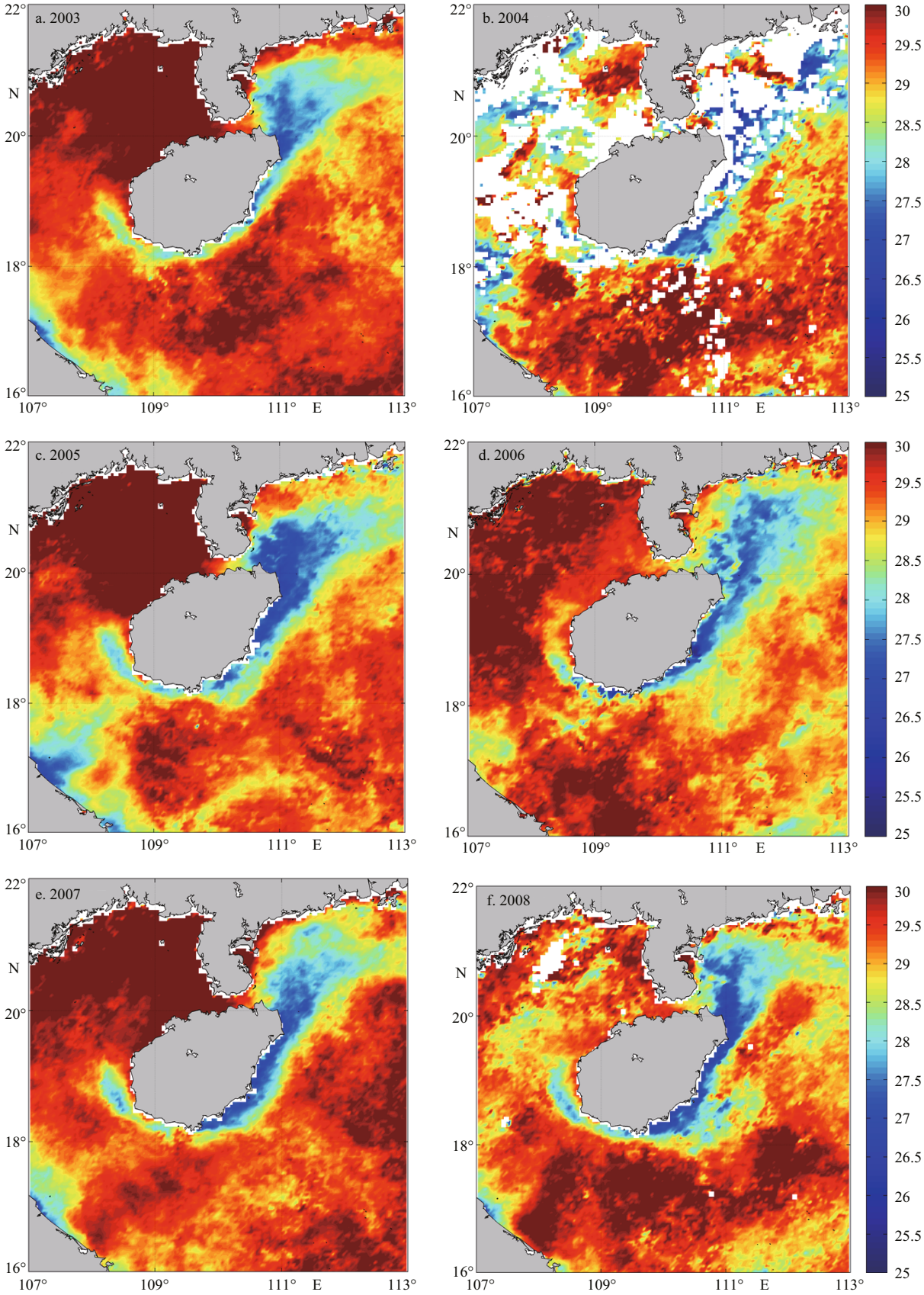

Fig.3 Monthly-mean SSTs (°C) from MODAS in July of 2003 to 2008

was obtained from 100 CTD profiles taken at a depth of 0.2 m. A large area of cold water with temperatures 4°C lower than that in the surrounding area is seen northeast of Hainan Island. The vertical temperature profile along section S1 (Fig.5a) shows that the temperature contour of 24°C intersects the surface near Station 4 and the SST between Stations 3 and 5 is below 26°C, indicating a seawater uplift near Station 4. Along S2 (Fig.5b), the 26°C contour intersects the surface near Station 3, showing another seawater uplift.

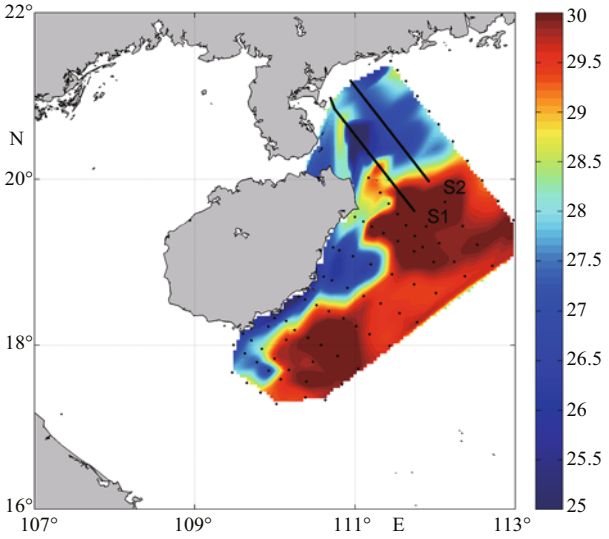

Fig.4 In-situ temperature distribution (°C) at a depth of 0.2 m

In-situ data were collected from July 19 to August 5, 2006. The solid black dots denote the locations of 100 survey stations, and the two lines S1 and S2 denote the positions of the Transects referred to in Fig.5.

All the above analyses based on satellite data, MODAS, and in-situ observations indicate that significant upwelling occurs east-northeast of Hainan Island during summertime.

3 NUMERICAL MODEL AND EXPERIMENT CONFIGURATION

3.1 High-resolution nested ocean model

The Princeton Ocean Model (POM) 2002 version (referred to as pom2k) was used in this study. It is a three-dimensional, primitive equation ocean model that includes a simplified version of the level 2.5 Mellor and Yamada turbulent closure scheme (Mellor and Yamada, 1982; Mellor, 1989). We employed the nested technique in the configuration (Fig.1). The outer domain covers the entire SCS with a resolution of 1/8°, while the inner domain envelopes the whole of Hainan Island as well as its coastal regions with a fine resolution of 2 minutes (1/30°) which can resolve mesoscale processes on the continental shelf. The boundary of the nesting model was treated as follows. First, the depths of the inner domain grids along the boundary were set equal to the outer domain grids. Second, the currents, surface elevations, temperatures and salinities at the open boundaries of the inner domain were obtained by spatial (bilinear) interpolation of the model's monthly output from the outer domain. Finally, the normal external velocity was modified following Guo et al. (2003). The 2-min Earth Topography (ETOPO2.V2) (Marks and Smith, 2006) was used in this study. Tidal processes were not

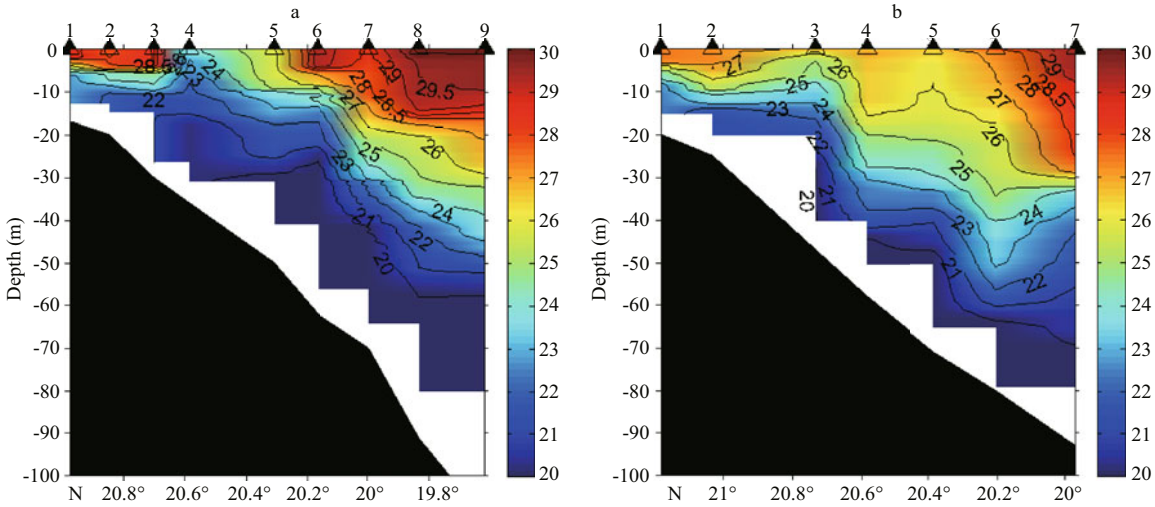

Fig.5 Vertical cross-sections of temperature (°C) along (a) S1 (9 stations) and (b) S2 (7 stations)

The locations of S1 and S2 are shown in Fig.4. The temperature data along S1 and S2 were collected during July 21–22, 2006.

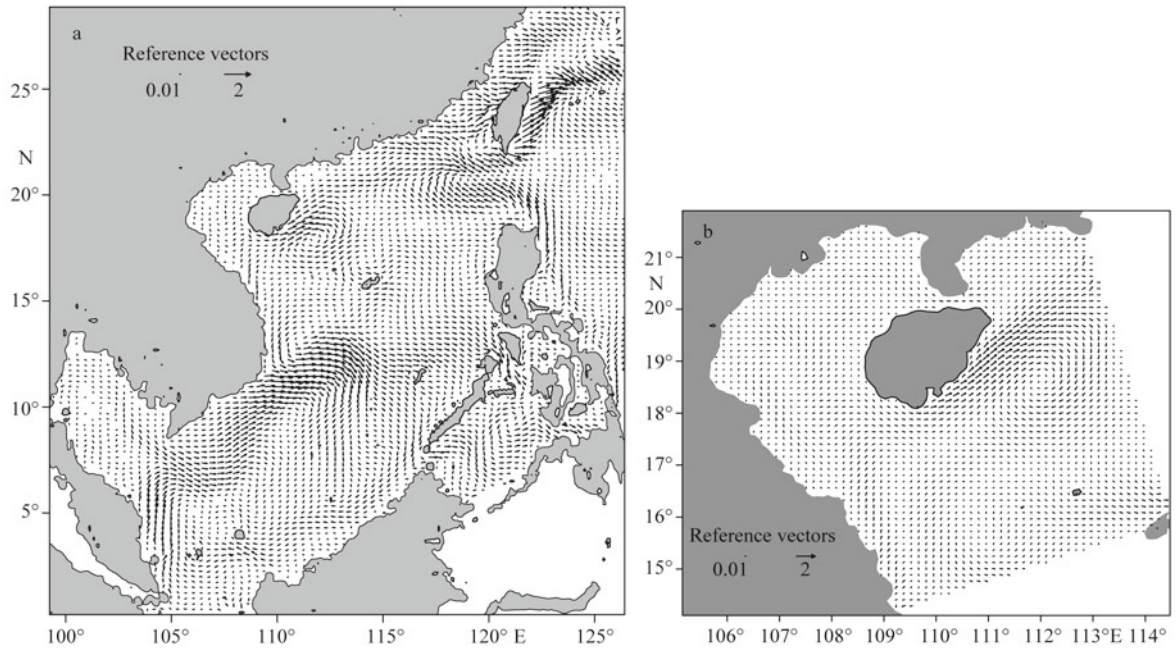

Fig.6 Horizontal distributions of modeled 8-year-averaged monthly-mean current vectors at a depth of 5 m in August for (a) the outer domain and (b) the inner domain (m/s)

considered in this study since they play a minor role in the upwelling process (Lee et al., 1999). The model uses a σ-coordinate with 23 layers in the vertical. Daily QuikSCAT surface winds from January averaged over 8 years (2000–2007) were used for spinning-up of the model. A 3-d mean of the daily QuikSCAT winds over 2000–2007 was used for the following simulation. The wind data has a spatial resolution of 0.25°. Other meteorological forcing data including net heat fluxes and short-wave radiation fluxes were obtained from the NCAR/NCEP reanalyses (Kalnay et al., 1996). The initial temperature and salinity were obtained from the WOA01 (World Ocean Atlas 2001) (Boyer et al., 2001). Simple Ocean Data Assimilation (SODA) data (Carton et al., 2000) were used for the open boundaries of the outer domain. The surface temperature and salinity were restored to the climatologically monthly mean with a time scale of 60 d.

A 10-year spin-up was performed using the climatologically mean QuikSCAT winds of January averaged from 8-year daily winds over 2000–2007. Subsequently, the model runs forward from 2000 to 2007 using the final output from the spin-up.

3.2 Design of the sensitivity experiments

As discussed in Section 1, the upwelling involves a few factors including winds, bottom topography, large-scale circulation, and mesoscale eddies. There may be different dynamic mechanisms for the upwelling occurring at different areas. In order to obtain a better understanding of the effects of the local wind stresses and large-scale circulation on the upwelling east and north of Hainan Island, five numerical experiments were designed as shown in Table 1. For the control run ("CNTR") of the experiment we forced 8-year-averaged (2000–2007) monthly-mean winds and outer domain currents in the open boundary in July. The relative standard deviation of the wind field during 2000–2007 in the inner domain was more than 0.5. Considering the stability of the calculation, we used $0.5\times U_w$ (U_w refers to the 8-year-averaged monthly-mean winds in the inner domain) for the case of a weak winds year ("Wind_1") and $1.5\times U_w$ for a strong wind year ("Wind_2"). The relative standard deviation of the open boundary currents of the inner domain during 2000–2007 did not exceed 0.2. Thus, we used $0.8\times U_o$

Table 1 Design of the sensitivity experiments

Experiment name	CNTR	Wind_1	Wind_2	BC_1	BC_2
Wind	U_w*	$U_w\times0.5$	$U_w\times1.5$	U_w	U_w
Boundary currents	U_o**	U_o	U_o	$U_o\times0.8$	$U_o\times1.2$

* U_w denotes the 8-year-averaged monthly mean wind force in July;
** U_o denotes the open boundary currents from the outer domain.

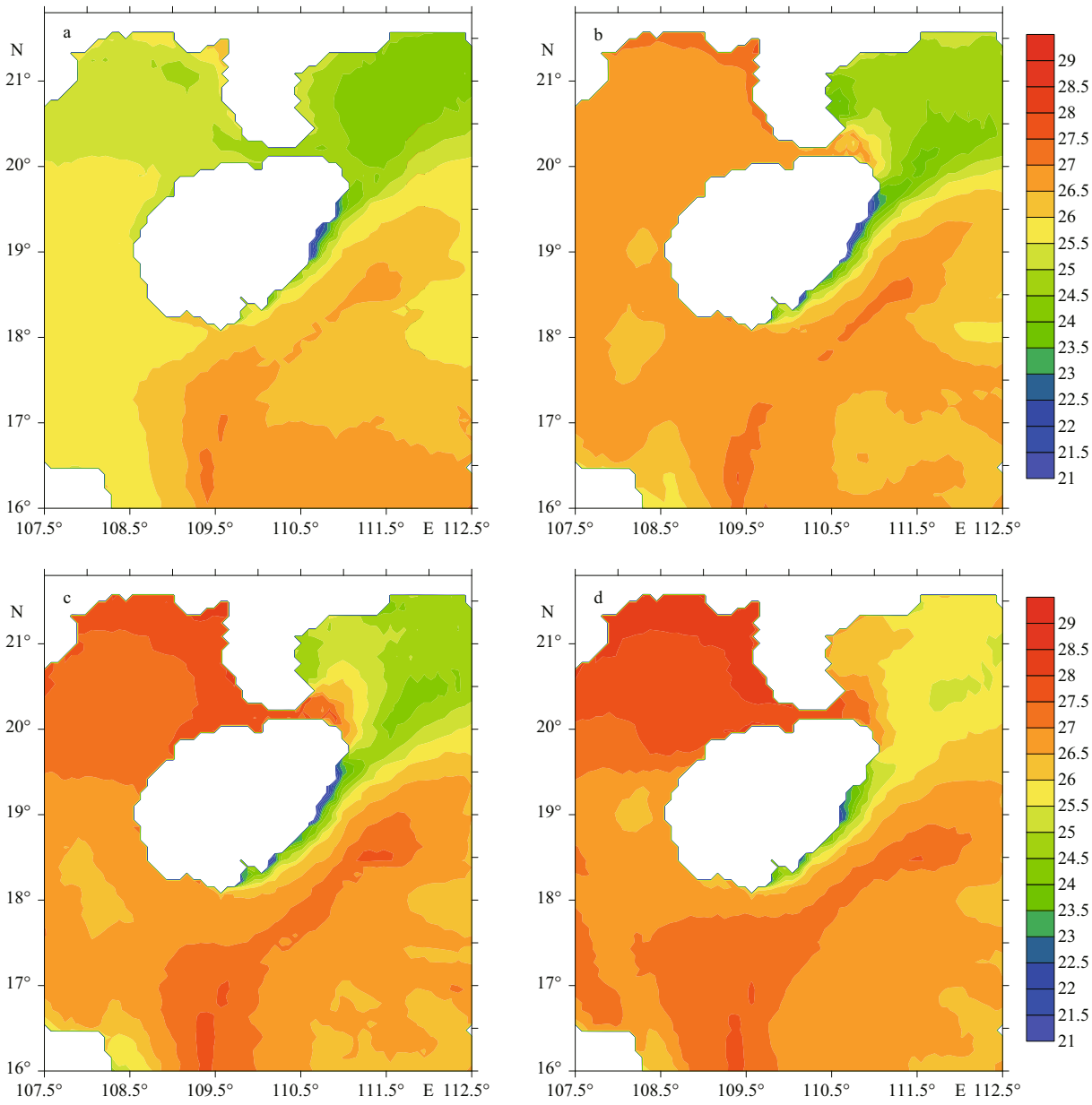

Fig.7 Modeled results of 8-year-averaged monthly-mean sea temperature at a depth of 5 m in the continental shelf of the northern South China Sea in (a) June; (b) July; (c) August; and (d) September

(U_o refers to the 8-year-averaged monthly-mean outer domain currents in the inner domain open boundary) for the case of a weak large-scale circulation year ("BC_1") and $1.2\times U_o$ for a strong large-scale circulation year. The purpose of these experiments was to investigate the sensitivity of the upwelling intensity to the local wind and large-scale circulation. For this purpose, when changing the local winds or boundary currents in the experiment, other computational conditions (e.g., the surface heat forcing) remained constant. All experiments started on July 1, 2000 and ran 10 days forward in time.

4 EXPERIMENTAL RESULT

4.1 Upwelling analysis from model outputs

Figure 6a and b illustrate the 8-year-averaged (2000–2007) monthly-mean currents at a depth of 5 m in August in the outer domain and inner domain, respectively. The key characteristics of the main currents in the SCS are shown in Fig.6a. Strong northeasterly currents flow along the east coast of Hunan Island with an anti-cyclonic eddy centered east and southeast of the island (Fig.6b). Figures 7

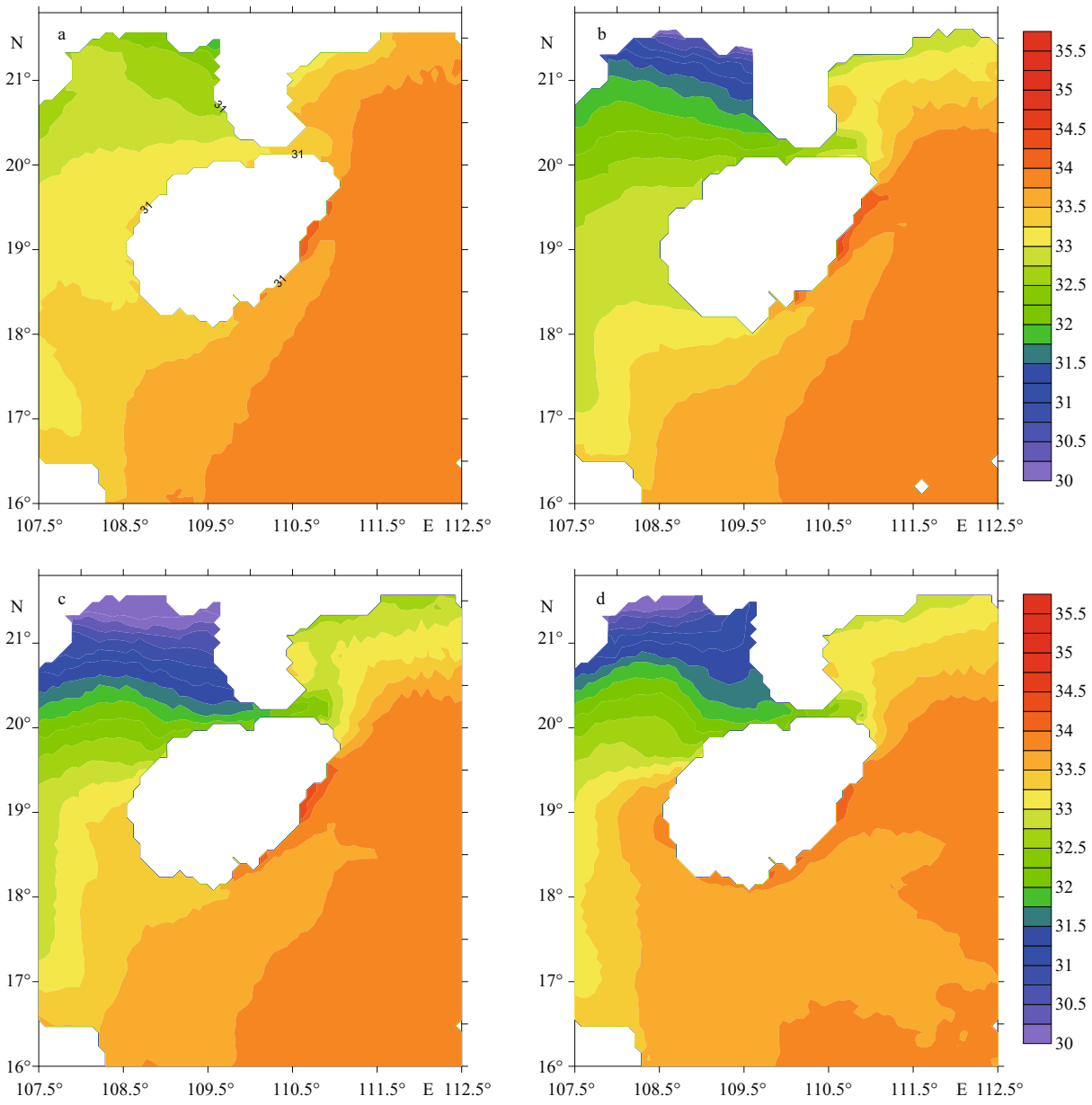

Fig.8 Same as Fig.7, except for the salinity

and 8 show the 8-year-averaged monthly-mean sea temperature and salinity, respectively, at a depth of 5 m from June to September. Cold water (Fig.7) with high salinity (Fig.8) can be found east and northeast of the island during this period, indicating that the upwelling occurred in June and lasted until September. The intensity of the upwelling reached its peak in July when observations showed the largest area of cold water extending to the northeastern offshore regions. The model results agree qualitatively with the satellite SSTs shown in Figs.2 and 3, indicating that the model reproduces the upwelling processes east and northeast of the island.

In order to quantify the variation of the upwelling intensities, we define the parameter Δt:

$$\Delta t = t_{150} - t_{30}, \quad (1)$$

where t_{150} and t_{30} are the sea temperatures at 5 m depth located at the same latitude but with a seafloor depth of 150 m and 30 m, respectively. Being at the same latitude, the two sites are likely to receive similar solar radiation; thus, the differences of the 5-m sea temperatures between the two sites would be caused primarily by upwelling processes and/or horizontal advection. Figure 9 shows the variation of the 8-year-mean Δt, relative vorticity, and offshore velocity at Site 1 (Fig.1b) from June 1 through September 30.

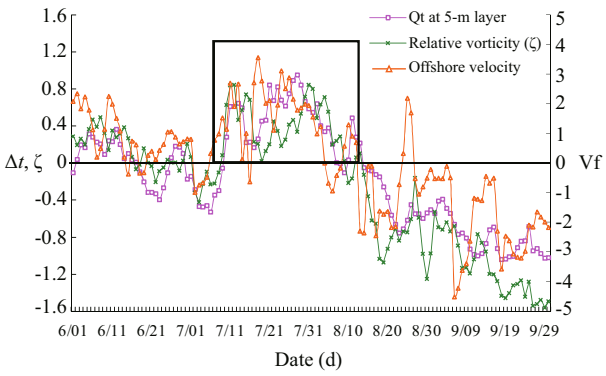

Fig.9 The variation of the normalized 8-year-averaged Δ*t* (°C), relative vorticity (m/s²), and offshore velocity (m/s) from June 1 to September 30

The black box indicating the episode of strong upwelling from mid-July to mid-August.

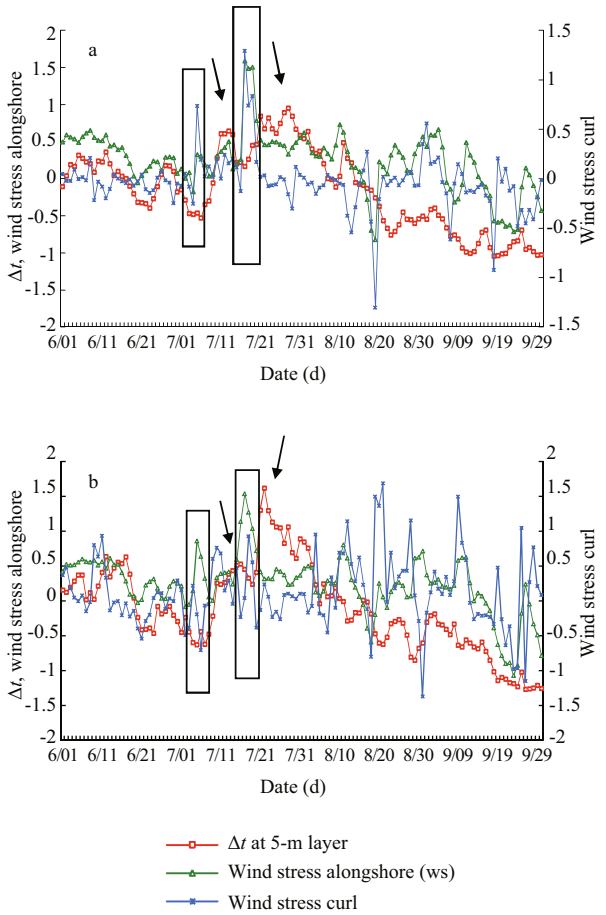

Fig.10 Variations of the normalized 8-year-averaged Δ*t* (°C), alongshore wind stress (N/m²), and wind stress curl (N/m³) from June 1 to September 30 in (a) Site 1; (b) Site 2 (indicated in Fig.1b)

Two episodes of strong upwelling are marked with black boxes (enveloping the peaks of alongshore wind stress), with black arrows indicating the peaks of Δ*t*.

Because the orders of magnitude of these three parameters are quite different, we normalized their values using the following method

$$cx_i = \frac{(X_i - X_{\text{mean}})}{X_{\text{mean}}} \qquad i = 1, 2, \cdots, n$$

$$X_{\text{mean}} = \frac{\sum_1^n X_i}{n} \tag{2}$$

where cx is the normalized data, X_i is the original data and X_{mean} is the mean value of the data set. The three parameters in Fig.9 have similar trends of variation, with a correlation coefficient of 0.887 between Δ*t* and the relative vorticity and 0.762 between Δ*t* and the offshore velocity. Wind-induced Ekman transport causes offshore surface flow and vertical transportation in the coastal area. In this case, the vertical component of the relative vorticity and the offshore velocity in the upper ocean in the coastal area are highly correlated with the upwelling intensity. Thus, the high correlation coefficients between Δ*t* and the relative vorticity and offshore velocity indicate that the time series of Δ*t* can be used as an index of the upwelling intensity in this region. The variation of Δ*t* clearly shows a period of strong upwelling from July 11 through August 13. After August 13, the upwelling process weakened rapidly.

Figure 10a, b shows the variations of the normalized 8-year-mean Δ*t*, wind stress along the shore, and wind stress curl along the east coast of Hainan Island from June 1 to September 30 at Sites 1 and 2 (Fig.1b), respectively. At Site 1 (Fig.10a) the variations of the wind stress curls and the alongshore wind stresses are synchronous, while the variation of Δ*t* lags 3–5 d behind them. A correlation analysis shows that the 4-d-lagged correlation coefficient between Δ*t* and the alongshore wind stresses has a maximum value of 0.621, while that between Δ*t* and the wind stress curl reaches 0.353. The higher 4-d-lagged correlation between Δ*t* and the alongshore wind stresses at Site 1 implies that the intensity of the upwelling east of the island was influenced primarily by the alongshore wind stresses. For Site 2 (Fig.10b), the results are similar, with a 5-d-lagged correlation between Δ*t* and the alongshore wind stress (or wind stress curl) reaching a maximum value of 0.681 (or 0.156). The correlation between Δ*t* and the wind stress curl at Site 2 was lower than at Site 1, indicating that the wind stress curl had less influence on the upwelling intensity at Site 2. A further comparison between Fig.10a and b shows that the maximum Δ*t* on the

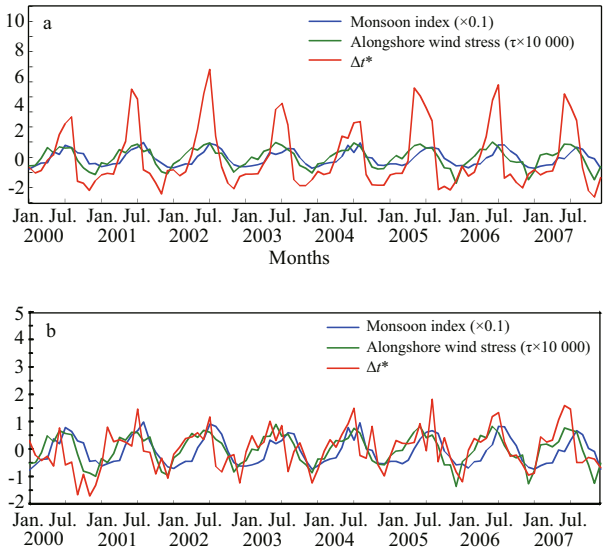

Fig.11 Variations of monthly-mean Δ*t* anomaly Δ*t ($\Delta t^* = \Delta t - \overline{\Delta t}$ °C), alongshore wind stress (N/m²×10 000) and SEASM index (m/s×0.1) at (a) Site 1 and (b) Site 2 (indicated in Fig.1b)**

For comparison, the alongshore wind stresses are multiplied by a factor of 10 000.

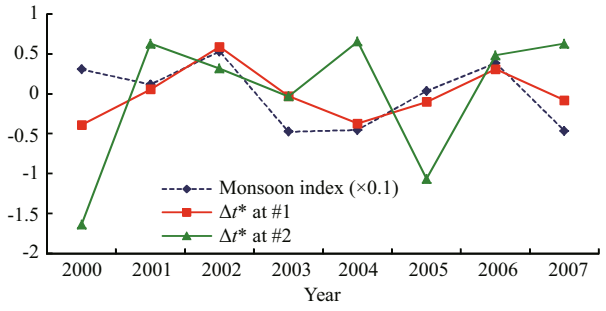

Fig.12 Variations of the normalized SEASM index (m/s×0.1), Δ*t* anomalies Δ*t (°C) at Site 1 and Site 2 on July of 2000 to 2007**

northeast coast (Site 2) occurred 1 d after that on the east coast (Site 1), implying that the cold water in the northeast coast may be partially transported from the east coast by the alongshore currents (Fig.4).

4.2 Inter-seasonal/inter-annual variations of the upwelling and their correlations with the South China Sea and the East Asian Summer Monsoons

The results presented in the previous section indicate that the upwelling that occurred east of the island was primarily driven by the alongshore winds which may be associated with the South China Sea and the East Asian Summer Monsoons (SEASMs). It is thus of interest to examine the relationship between the inter-annual variation of the upwelling and that of the SEASM. Here, we employ a SEASM index calculated using the averaged zonal wind velocity $\overline{U}$ in the area 5°–15°N，110°–120°E (Wang et al., 1999, 2004). This index represents the intensity of SEASM. Figure 11 shows the monthly variations of the Δt anomalies ($\Delta t^* = \Delta t - \overline{\Delta t}$, $\overline{\Delta t}$ refers to the 8-years averaged Δt of a single month), alongshore wind stresses, and SEASM index at Site 1 and Site 2 (Fig.1b). The inter-seasonal variations of the Δt anomalies, alongshore wind stresses, and SEASM index are clearly displayed at both Site 1 and Site 2, with peaks in the summers and lows in the winters. The Δt anomaly also shows inter-annual variations at Site 1, with the strongest occurring in 2002 and the weakest in 2004, but no obvious inter-annual variation is found at Site 2. The variation of the Δt anomalies and the alongshore wind stresses is highly correlated with that of the SEASM index for both sites with a lag of about one month. This one-month-lagged correlation coefficient at Site 1 is as high as 0.835, although the inter-annual variation of the SEASM index does not seem significant. The correlation coefficients between the Δt anomalies and the alongshore wind stresses reach maximum values of 0.786 for Site 1 and 0.618 for Site 2 indicating that the role of the alongshore winds in driving the upwelling at Site 2 is not as large as that at Site 1. Since both the intensity of the upwelling and that of SEASM reached their maximum values around July, we compared the inter-annual variations of Δt anomalies and the normalized SEASM index at Site 1 and Site 2 in July from 2000 to 2007 (Fig.12).

At Site 1, the trend of inter-annual variation of the Δt anomalies is similar to that of the SEASM index, with maximum values in 2002 and 2006 and minimum ones in 2003 and 2004. At Site 2, however, the variation trend of Δt anomalies is quite different to that of the SEASM index. The results imply that the inter-annual variation of the upwelling east of Hainan Island is controlled primarily by the East Asian Summer Monsoon system while that of the upwelling northeast of the island may be determined by other factors in addition to the monsoons. Figures 13–14 display the distribution of the correlation coefficient between sea temperature and area-averaged zonal/meridional velocity anomalies at a depth of 5 m in July and August. A large negative correlation is seen offshore northeast of the island, which indicates that the large-scale circulation plays an important role in the intensity of the upwelling northeast of the island.

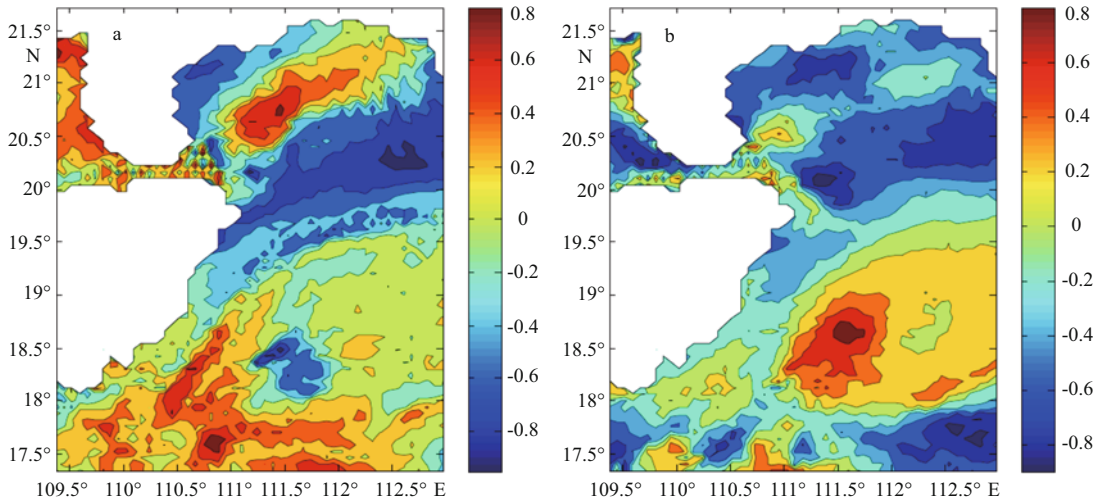

Fig.13 Distribution of correlation coefficient between sea temperature anomaly and zonal velocity anomaly at a depth of 5 m in (a) July and (b) August

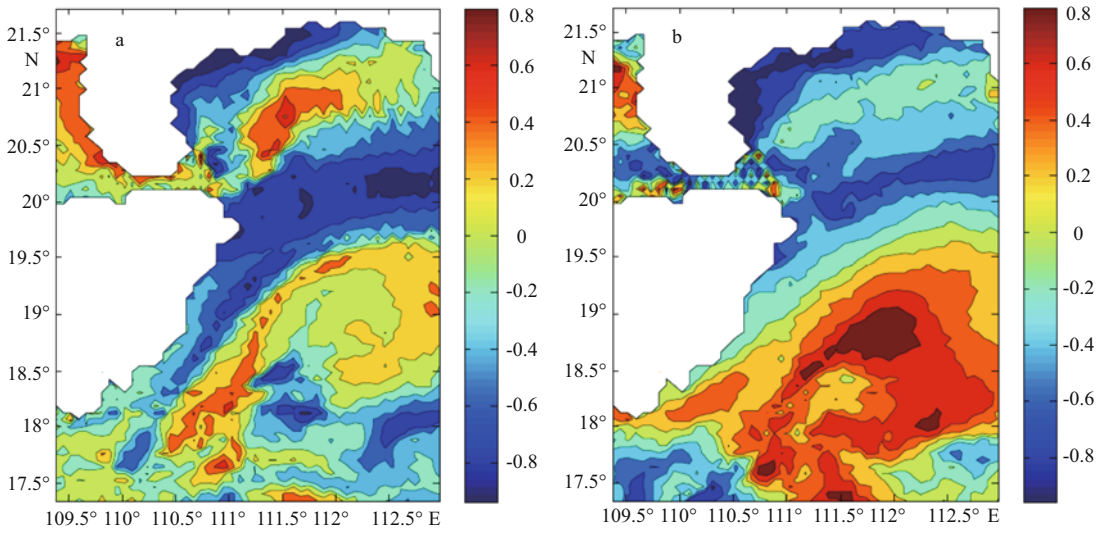

Fig.14 Distribution of correlation coefficient between sea temperature anomaly and meridional velocity anomaly at the 5-m layer in (a) July and (b) August

4.3 Sensitivity experiments

To evaluate the relative importance of the wind stresses and the large-scale circulation in the upwelling regions east and northeast of the island, we performed five sensitivity experiments by enhancing/weakening the wind stresses or the large-scale circulation (Table 1). As discussed in section 4.1, the variation of upwelling intensity lags 3–5 d behind that of the alongshore wind stresses. Therefore, we analyzed the model output on the 4th day of integration. Figure 15 shows the difference in sea temperatures and currents between the sensitivity experiments and the control run at a depth of 5 m. When the wind stresses are weakened (Wind_1) or enhanced (Wind_2), the temperatures become higher or lower, respectively, at both the east and the northeast coasts of the island, accompanied by an onshore or offshore current anomaly (Fig.15a, b). This result indicates that the local wind stress is a major factor in the upwelling process east of the island. On the other hand, when the large-scale circulation is weakened (BC_1) or enhanced (BC_2) at the open boundary (Fig.15c, d), warmer or colder water is found northeast of the island, respectively. The vertical cross-section of the seawater velocity differences between BC_2 and the control run along line 1 (Fig.16) also indicates that an enhanced large scale circulation at the open

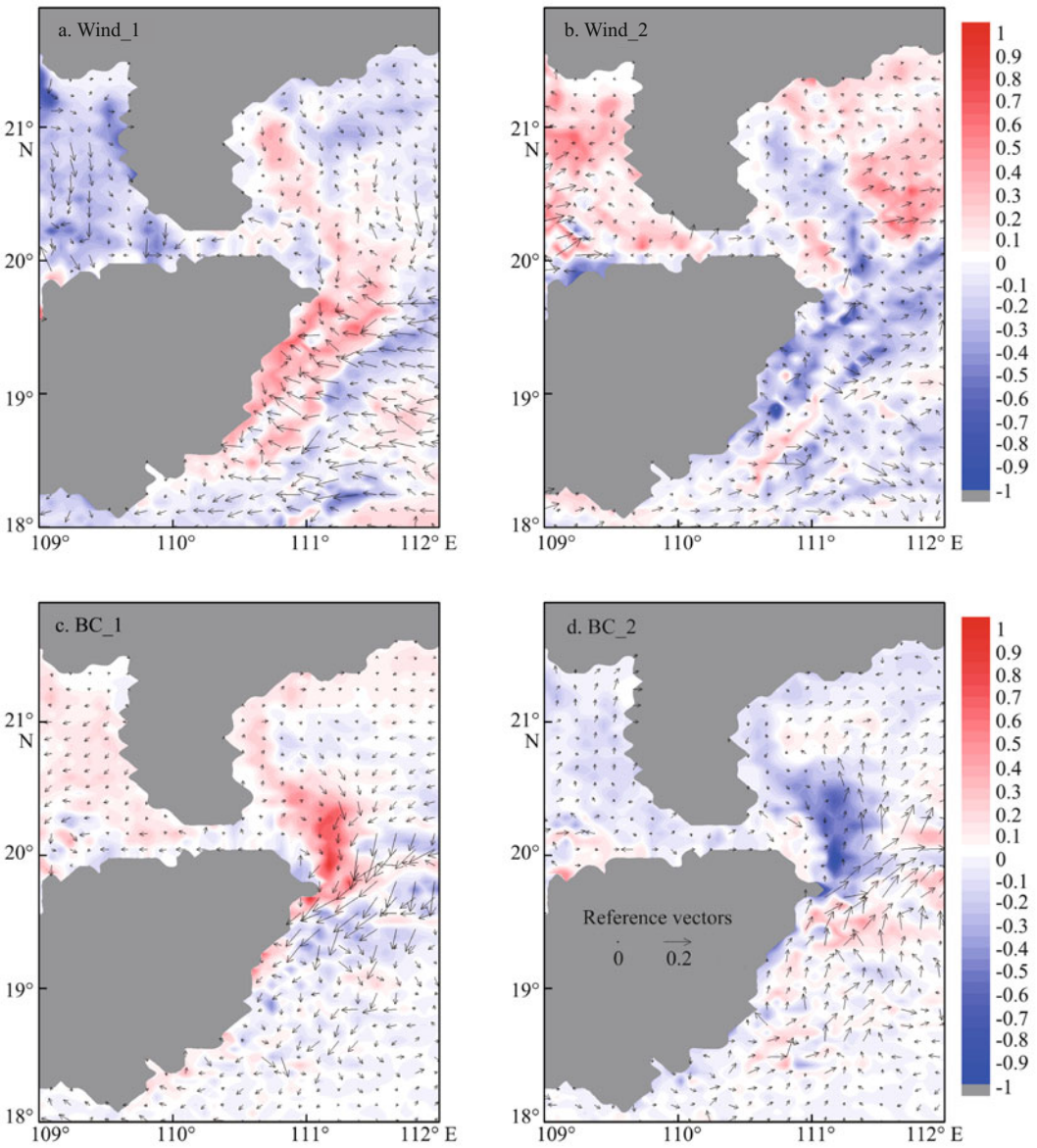

Fig.15 Distribution of sea temperature (°C) and current (m/s) differences between sensitivity experiments of (a) Wind_1; (b) Wind_2; (c) BC_1; (d) BC_2 and the control run at a depth of 5 m

boundaries can induce or intensify the upwelling northeast of the island. In this process, the large-scale circulation flows along the isobaths in the form of an alongshore current along the east coast of the island and then changes to an offshore current when it reaches the northeast coast. This indicates that the submarine topography is significant in this process. Therefore, the large-scale circulation, which flows northeastward along the east coast of the island and becomes offshore currents at the northeastern coast, may play a vital role in the generation or intensification of the upwelling northeast of the island.

Comparing the Wind_2 and BC_2 experiments, we find that the wind stress gives rise to the upwelling off both the east and the northeast coasts while the large scale circulation causes the upwelling off the northeast coast. Furthermore, the alongshore circulation transports the cold water northeastward from the east coast to the northeast coast. As a result of the combining effects of the wind stresses and the large scale circulation, the water off the northeast coast is colder and the cold area is much larger in size than that off the east coast, in agreement with the satellite SSTs shown in Figs.2 and 3.

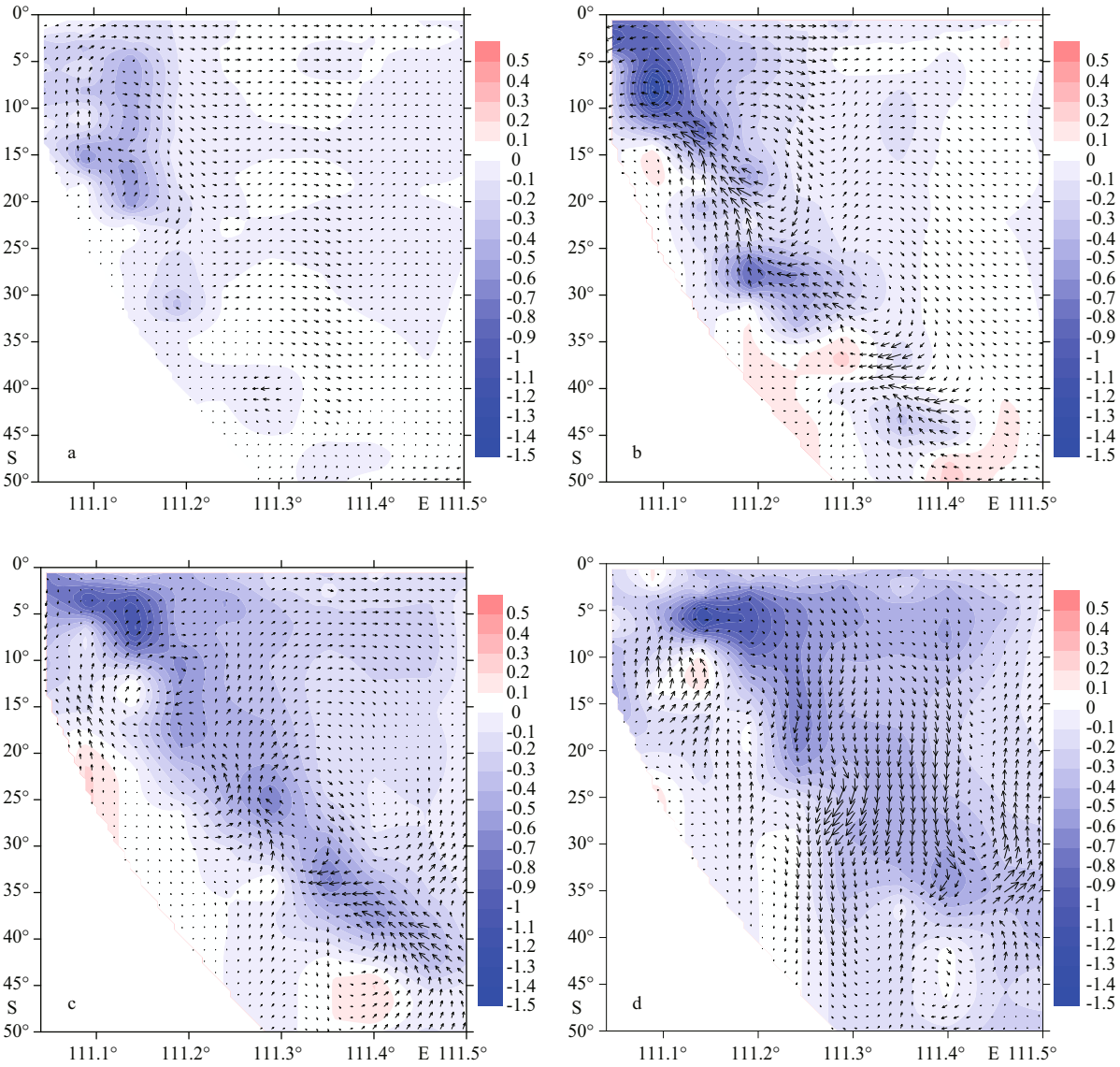

Fig.16 Vertical distribution of the differences in velocity (*u* and *w* components) and sea temperature (°C) between sensitivity experiment BC_2 and the control run along line 1 for (a) 1 d; (b) 2 d; (c) 3 d; and (d) 4 d simulation

The position line 1 is indicated in Fig.1b; the vertical velocity has been amplified 1 000 times for plotting the vectors.

5 CONCLUSION

A 3-D nested POM forced by QuikSCAT winds was employed to simulate the summer upwelling east and northeast of Hainan Island. The results indicate that the model can reproduce the main features of the upwelling. The strongest upwelling processes were found during the period of July 11 through August 13. The inter-annual variation of the upwelling east of the island has a similar trend to that of the East Asian Summer Monsoon system, but such a trend is not found in the upwelling northeast of the island.

The results from a set of sensitivity experiments further confirm that the upwelling east of the island is caused primarily by the alongshore wind stresses, while the upwelling northeast of the island is caused by both the alongshore wind stresses and the large-scale circulation. The large-scale circulation flowing northeastward along the east coast transports cold water from the south and turns offshore off the northeast coast; this process uplifts water mass from the bottom layer near the shore. We suggest that this process is the cause of the large area of cold water found off the northeastern coast. Nevertheless, the summer upwelling around the island is a very complex hydrodynamic process, which may be associated with other factors that are not considered here such as tides and waves. We plan to conduct further experiments in

the future in order to get a better understanding of the mechanism of the upwelling and its maintenance .

References

Barber R T, Chavez F P, Kogelschatz J E. 1985. Biological effects of El Niño. *In*: Vegas M ed. Seminario Regional Ciencas Tecnologiay Agression Ambiental: El Fenomeno "El Niño". Contec Press, Lima, Peru. p.399-438.

Boyer T P, Stephens C, Antonov J I, Conkright M E, Locarnini R A, O'Brien T D, Garcia H E. 2002. *In*: Levitus S ed. World Ocean Atlas 2001. Vol.1: Salinity. NOAA Atlas NESDIS 50, US Government Printing Office, Washington, DC. p.176-182.

Carton J A, Chepurin G, Cao X, Giese B. 2000a. A simple ocean data assimilation analysis of the global upper ocean 1950–1995 Part I: Methodology. *J. Phys. Oceanogr.*, **30**: 294-309.

Carton J A, Chepurin G, Cao X. 2000b. A simple ocean data assimilation analysis of the global upper ocean 1950–1995 Part II: Results. *J. Phys. Oceanogr.*, **30**: 311-326.

Chai F, Xue H, Shi M. 2001. Upwelling east of Hainan Island. *Oceanogr. China*, **13**: 129-137.

Deng S, Zhong H L. 1995. On relation between upwelling off Qionghai and fishery. *Journal of Oceanography in Taiwan Strait*, **14**(1): 51-56. (in Chinese)

Ekman V W. 1905. On the influence of the Earth's rotation on ocean currents. *Arch. Math. Astron. Phys.*, **2**(11): 1-52.

Guan B X, Chen S J. 1964. Ocean Current System in East China Sea and South China Sea. Qingdao, Institute of Oceanology, Chinese Academy of Sciences. (in Chinese)

Guo F, Si M C, Xia Z W. 1998. Two-dimension diagnose model to calculate upwelling on offshore of the east coast of Hainan Island. *Acta Oceanologica Sinica*, **20**: 109-116. (in Chinese)

Guo X Y, Hisashi H, Yasumasa M, Toshio Y. 2003. A triply nested ocean model for simulating the Kuroshio-roles of horizontal resolution on JEBAR. *J. Phys. Oceanogr.*, **33**: 146-169.

Han W Y, Wang M B, Ma K B. 1990. The lowest surface water temperature area of China Sea in summer—the upwelling along the east coast of Hainan Island. *Oceanologia et Limnologia Sinica*, **21**: 167-275. (in Chinese)

Hong Q M, Li L. 1991. A study of upwelling over continental shelf off eastern Guangdong. *Journal of Oceanography in Taiwan Strait*, **10**(3): 272-277. (in Chinese)

Jing Z Y, Qi Y Q, Hua Z L, Zhang H. 2009. Numerical study on the summer upwelling system in the northern continental shelf of the South China Sea. *Continental Shelf Research*, **29**: 467-478.

Kalnay E, Kanamitsu M, Kistler R, Collins W, Deaven D, Gandin L, Iredell M, Saha S, White G, Woollen J, Zhu Y, Leetmaa A, Reynolds R, Chelliah M, Ebisuzaki W, Higgins W, Janowiak J, Mo K C, Ropelewski C, Wang J, Roy J, Dennis J. 1996. The NCEP/NCAR 40-year reanalysis project. *Bull. Am. Meteorol. Soc.*, **77**(3): 437-471, http://dx.doi.org/10.1175/1520-0477(1996)077.

Kara A B, Barron C N. 2007. Fine-resolution satellite-based daily sea surface temperatures over the global ocean. *J. Geophys. Res.*, **112**: C05041, http://dx.doi.org/10.1029/2006JC004021.

Lee H J, Chao S Y, Fan K L, Kuo T Y. 1999. Tide-induced eddies and upwelling in a semi-enclosed basin: Nan Wan. *Estuarine Coastal Shelf Science*, **49**(6): 775-787, http://dx.doi.org/10.1006/ecss.1999.0524.

Li L. 1990. A study on the summer upwellings in shelf waters west to Zhujiang River mouth. *Journal of Oceanography in Taiwan Strait*, **4**: 338-346. (in Chinese)

Li L. 1993. Summer upwelling system over the northern continental shelf of the south China Sea—physical description. Proceedings of the Symposium on the Physical and Chemical Oceanography of the China Seas. China Ocean Press, Beijing. p.58-68.

Liu K, Chao S Y, Shaw P T, Gong G C, Chen C C, Tang T Y. 2002. Monsoon-forced chlorophyll distribution and primary production in the South China Sea: observational and a numerical study. *Deep-Sea Research*, **49**(8): 1 387-1 412.

Marks K M, Smith W H F. 2006. An evaluation of publicity available global bathymetry grids. *Marine Geophysical Researches*, **27**: 19-34.

Mellor G L, Yamada T. 1982. Development of a turbulence closure model for geophysical fluid problems. *Rev. Geophys. Space Phys.*, **20**: 851-875.

Mellor G L. 1989. Retrospect on oceanic boundary layer modeling and second moment closure. *In*: Hawaiian Winter Workshop on "Parameterization of small-scale processes", January, University of Hawaii, Honolulu, Hawaii.

Niino H, Emery O. 1961. Sediment of shallow portions of East China Sea and South China Sea. *Geological Society of American Bulletin*, **72**: 731-761.

Su J, Pohlmann T. 2009. Wind and topography influence on an upwelling system at the eastern Hainan coast. *Journal of Geophysical Research*, **114**: C06017.

Su J L. 2004. Overview of the South China Sea circulation and its influence on the coastal physical oceanography outside the Pearl River Estuary. *Continental Shelf Research*, **24**: 1 745-1 760.

Wang B, Fan Z. 1999. Choice of south Asian summer monsoon indices. *Bulletin of the American Meteorological Society*, **80**(4): 629-638.

Wang B, Ho L, Zhang Y S, Lu M M. 2004. Definition of South China Sea monsoon onset and commencement of the East Asia summer monsoon. *Journal of Climate*, **17**: 669-710

Wyrtki K. 1961. Physical oceanography of the Southeast Asia waters. *NAGA Report*, **2**: 1-195.